Physics and Chemistry of Minerals
https://doi.org/10.1007/s00269-019-01023-3

ORIGINAL PAPER

Equations of state of Co_2TiO_4-Sp, Co_2TiO_4-CM, and Co_2TiO_4-CT, and their phase transitions: an experimental and theoretical study

Yanyao Zhang[1,2] · Xi Liu[1,2] · Sean R. Shieh[3] · Zhigang Zhang[4] · Xinjian Bao[1,2] · Tianqi Xie[3] · Fei Wang[1,2] · Clemens Prescher[5] · Vitali B. Prakapenka[5]

Received: 20 March 2017 / Accepted: 29 January 2019

Abstract

Co_2TiO_4 spinel (Co_2TiO_4-Sp) was synthesized at 1573 K and room P by heating in an argon atmosphere for 72 h, and quasi-hydrostatically compressed to ~ 24 GPa using a diamond-anvil cell in conjunction with a synchrotron X-ray radiation (ambient T). We found that the Co_2TiO_4-Sp was stable up to ~ 21 GPa and transformed to a new phase at higher P. With some theoretical simulations, we revealed that this new phase adopted the $CaMn_2O_4$-type structure (Co_2TiO_4-CM), which might further transform to the $CaTi_2O_4$-type structure (Co_2TiO_4-CT) at ~ 35 GPa. The isothermal bulk modulus (K_T) was experimentally obtained as 175.5(36) GPa for the Co_2TiO_4-Sp and 161(7) GPa for the Co_2TiO_4-CM, with its first pressure derivative K_T' as 2.8(5) and 7.3(8), respectively. Furthermore, the K_T was theoretically constrained (the GGA method) as 138(3) GPa for the Co_2TiO_4-CM and 196.8(14) GPa for the Co_2TiO_4-CT, with the K_T' as 7.6(3) and 5.0(1), respectively. Consequently, the Co_2TiO_4-CM is ~ 12.3% denser than the Co_2TiO_4-Sp at ~ 21 GPa, whereas the Co_2TiO_4-CT is just ~ 0.8% denser than the Co_2TiO_4-CM at ~ 35 GPa. The spinel and post-spinel phase assemblages for the Co_2TiO_4 composition at some high T have been tentatively deduced as Co_2TiO_4-Sp, CoO-B1 (NaCl-type structure) + $CoTiO_3$-Ilm (ilmenite-type structure), 2CoO-B1 + TiO_2-α-PbO_2 (α-PbO_2-type structure), Co_2TiO_4-CM and Co_2TiO_4-CT, as P increases.

Keywords Co_2TiO_4-CM · Co_2TiO_4-CT · Co_2TiO_4-Sp · DFT calculation · Diamond-anvil cell · Equation of state · High-P phase transition · Synchrotron X-ray diffraction

Introduction

The Co_2TiO_4 composition commonly crystallizes to a 4–2 inverse spinel (Co_2TiO_4-Sp; Romeijn 1953), which has interesting and useful electrical, magnetic, and electronic properties (Sakamoto 1962; Dube and Darshane 1991; Prosnikov et al. 2016). In Earth sciences, titanate spinels (A_2TiO_4-Sp) are conventionally considered as low-P analogues of the ringwoodite (Millard et al. 1995; Wang et al. 2002; Zhang et al. 2017), the most abundant mineral in the lower part of the mantle transition zone [ideally simplified as Mg_2SiO_4; e.g., Ringwood and Reid (1968), Irifune and Ringwood (1987), Ita and Stixrude (1992), and Frost (2008)]. It is therefore expected that the high-P behavior of the Co_2TiO_4-Sp may have some important implications on the high-P behavior of the Mg_2SiO_4 composition (Liebermann et al. 1977; Zhang et al. 2017).

The A_2TiO_4-Sp include Mg_2TiO_4-Sp, Mn_2TiO_4-Sp, Fe_2TiO_4-Sp, Co_2TiO_4-Sp and Zn_2TiO_4-Sp, which usually attain the inverse spinel structure at ambient conditions

Electronic supplementary material The online version of this article (https://doi.org/10.1007/s00269-019-01023-3) contains supplementary material, which is available to authorized users.

✉ Xi Liu
xi.liu@pku.edu.cn

1 Key Laboratory of Orogenic Belts and Crustal Evolution, MOE, Peking University, Beijing 100871, People's Republic of China

2 School of Earth and Space Sciences, Peking University, Beijing 100871, People's Republic of China

3 Department of Earth Sciences, University of Western Ontario, London, ON N6A 5B7, Canada

4 Key Laboratory of Earth and Planetary Physics, Institute of Geology and Geophysics, Chinese Academy of Sciences, Beijing 100029, People's Republic of China

5 Center for Advanced Radiation Sources, University of Chicago, Chicago, IL 60439, USA

Published online: 01 February 2019

[space group $Fd\bar{3}m$, No. 227; $Z=8$; structurally written as $(A^{2+})(A^{2+}Ti^{4+})O_4$; e.g., Verwey and Heilmann (1947), Sakamoto (1962), Hagenmuller et al. (1966), Wechsler and Von Dreele (1989), Dube and Darshane (1991), Sedler et al. (1994), Millard et al. (1995), Yamanaka et al. (2013)]. A large number of phase transitions have been reported for the A_2TiO_4-Sp. For example, the Fe_2TiO_4-Sp transforms to an Fe_2TiO_4-TDS phase (tetragonal distorted structure) at ~9 GPa, which further transforms to a Fe_2TiO_4-CT phase ($CaTi_2O_4$-type structure) at ~16 GPa (ambient *T*; Yamanaka et al. 2009, 2013). Similarly, extensive experimental investigations with different techniques have been conducted to establish the equation of state of the A_2TiO_4-Sp at high pressure [ambient *T*; e.g., Liebermann et al. (1977), Wang et al. (2002), Yamanaka et al. (2009), Yamanaka et al. (2013), Xiong et al. (2015), Lv et al. (2016), Zhang et al. (2017)].

In this study, we focused on the high-*P* behavior of the Co_2TiO_4-Sp. We synthesized the Co_2TiO_4-Sp using a solid-state reaction method (ambient *P*), and compressed this material to ~24 GPa using a diamond-anvil cell (DAC) in conjunction with a synchrotron X-ray radiation (ambient *T*). The compression experiments indicated a new phase stable at $P>\sim21$ GPa. To determine the structure of this high-*P* phase, we conducted some theoretical simulations and found that this phase should adopt the $CaMn_2O_4$-type structure (Co_2TiO_4-CM). Our simulation also suggested that the Co_2TiO_4-CM would further transform to a Co_2TiO_4-CT phase at ~35 GPa. In addition, the compressional behaviors of the Co_2TiO_4-Sp, Co_2TiO_4-CM, Co_2TiO_4-CT were investigated and compared, and the sequence of the phase assemblages for the Co_2TiO_4 composition at high *P*-*T* conditions was tentatively deduced.

Experimental and simulating methods

The Co_2TiO_4-Sp was synthesized by a solid-state reaction method. We used the chemicals CoO (99.99% purity; Alfa Aesar) and TiO_2 (99.99% purity; Alfa Aesar) to prepare the starting material for the synthesizing experiment. We first dried these chemicals at 1 atm and 1373 K for 36 h under an argon environment; second weighed them according to the stoichiometry of the Co_2TiO_4-Sp and homogenized them into a mixture with an agate mortar under acetone, and third pressed this mixture into a pellet. The resulting pellet was placed in a platinum crucible and sintered with a muffle furnace, which was continuously fluxed with argon. The sample was heated at 1573 K for 72 h and then slowly cooled to room *T* at the rate of − 5 K/min. According to Sakamoto (1962), our synthetic product was expected to be pure Co_2TiO_4-Sp.

One small portion of the synthetic sample from the high-*T* synthesizing experiment was processed and characterized using a scanning electron microscope (Quanta 650 FEG) and an electron microprobe (EMP; JEOL JXA-8100). The rest of the sample was slowly ground down to a fine powder, which was first checked with a powder X-ray diffractometer (X'Pert Pro MPD system) at ambient *P*–*T* conditions, and later used in our high-*P* synchrotron X-ray diffraction experiments.

With a symmetrical DAC, we conducted the high-*P* synchrotron X-ray diffraction experiments (ambient *T*) at the beamline 13-ID-D of the GSECARS, Advanced Photon Source (APS), Argonne National Laboratory. The experimental techniques were similar to those used in our previous studies (e.g., Liu et al. 2011; He et al. 2012; Zhang et al. 2017). The powder sample was mixed with a trace amount of Au powder, and loaded into a rhenium gasket with a hole of 100 μm in diameter. We used neon as the pressure medium, a ruby sphere as the pressure marker (the ruby fluorescence method; Mao et al. 1978), and an incident synchrotron radiation beam of the wavelength of 0.3344 Å and the size of ~3 × 4 μm^2. Due to the small X-ray beam size and the small amount of admixed Au, the XRD peaks of the gold were not usually detected and not very useful for pressure determination (see later discussion). The sample-to-detector distance (246.4524 mm) and the orientation of the detector were calibrated using LaB_6. Each X-ray diffraction image was collected for about 30–120 s using an online CCD detector, and later integrated to derive the one-dimensional X-ray diffraction pattern using the Dioptas program (Prescher and Prakapenka 2015). We processed the XRD data using the PeakFit V4.12 software (SPSS Inc.), and derived the unit-cell parameters using the UnitCell program (Holland and Redfern 1997).

Our electronic structure calculations were carried out with the CASTEP code using the density functional theory (DFT; Hohenberg and Kohn 1964; Kohn and Sham 1965) and planewave pseudopotential technique (Payne et al. 1992). Taking into account the potential order–disorder phenomenon in the spinel structure, we constructed the initial structural model of the Co_2TiO_4-Sp according to Rankin et al. (2008), and the resulting structural model was similar to that for the Zn_2TiO_4-Sp depicted in Fig. 6b of Zhang et al. (2017). In addition, the initial structural model of the Co_2TiO_4-CT (space group *Bbmm;* $Z=4$), Co_2TiO_4-CM (space group *Pbcm;* $Z=4$), and Co_2TiO_4-CF ($CaFe_2O_4$-type structure; space group *Pnma;* $Z=4$) were from Bertaut and Blum (1956), Giesber et al. (2001), and Decker and Kasper (1957), respectively. To consider the magnetic ordering of these phases, we carried out spin-polarized calculations with initial ferromagnetic and antiferromagnetic structures (labeled as Sp-fm, CT-fm, CM-fm and CF-fm, and Sp-afm, CT-afm, CM-afm and CF-afm, respectively).

We treated the exchange–correlation interaction by the generalized gradient approximation (GGA) with the Perdew–Burker–Ernzerhof functional (PBE; Perdew et al. 1996), and used a convergence criterion of 10^{-6} eV/atom on the total energy in the self-consistent field calculations. The GGA + U method (Dudarev et al. 1998) was employed to deal with the strong correlation effect of the Co^{2+} electrons, and the value of the Hubbard U for the on-site Coulomb interaction in the localized d orbitals was set as 2.5 eV; the effects of different U values on the energies, lattice parameters, magnetic and electronic properties of the Co_2TiO_4-Sp can be found in the Supplementary Material. Subject to the unavailability of any experimental measurements to facilitate comparisons, it was assumed that a Hubbard U of 2.5 in combination with the GGA method would work well for all other Co_2TiO_4 phases. We employed the ultrasoft pseudopotentials for the O, Co, and Ti in the CASTEP's internal libraries of pseudopotentials to model the ion–electron interaction, and the planewave basis set with an energy cutoff of 380 eV to expand the electronic wave functions (Vanderbilt 1990; Kresse and Hafner 1994). The cutoff core radii were 0.70 Å for the O atom in the electronic configuration $2s^2 2p^4$, 1.70 Å for the Co atom in the electronic configuration $3d^7 4s^2$, and 1.50 Å for the Ti atom in the electronic configuration $3s^2 3p^6 3d^2 4s^2$. We set a k-point separation as 0.07 $Å^{-1}$ for all the phases so that the initial k-point grids were automatically generated as $2\times2\times2$, $2\times5\times1$, $5\times1\times1$, and $1\times1\times5$ (Monkhorst and Pack 1976) for the Co_2TiO_4-Sp, Co_2TiO_4-CF, Co_2TiO_4-CM and Co_2TiO_4-CT, respectively. The effects of using larger energy cutoff and denser k-point meshes on the calculated properties were tested and found as negligible. By minimizing the Hellmann–Feynman force on the atoms and simultaneously matching the stress on the unit cell to the target stress, the equilibrium lattice parameters and internal coordinates were fully relaxed until the total energy was minimized.

Result and discussion

Synthetic Co_2TiO_4-Sp

The electron back-scatter images of our synthetic product suggest that there is only one crystalline phase, with grain sizes ranging from a few micrometers to a few dozens of micrometers (Fig. 1). The ambient powder X-ray diffraction data indicate no impurity and confirm the expected cubic spinel structure. The EMP analyses (4 analyses) performed on our synthetic product suggest a chemical formula of $Co_{2.01(2)}Ti_{1.00(0)}O_{4.00}$, which is essentially identical to the ideal chemical formula of the Co_2TiO_4-Sp. The powder X-ray diffraction data at ambient conditions give out the unit-cell parameters of our Co_2TiO_4-Sp as $a_0 = 8.454(0)$ Å and $V_0 = 604.28(8)$ $Å^3$, in good agreement with those from Sakamoto (1962; $a_0 = 8.44$ Å) and Hirota et al. (1990; $a_0 = 8.443$ Å).

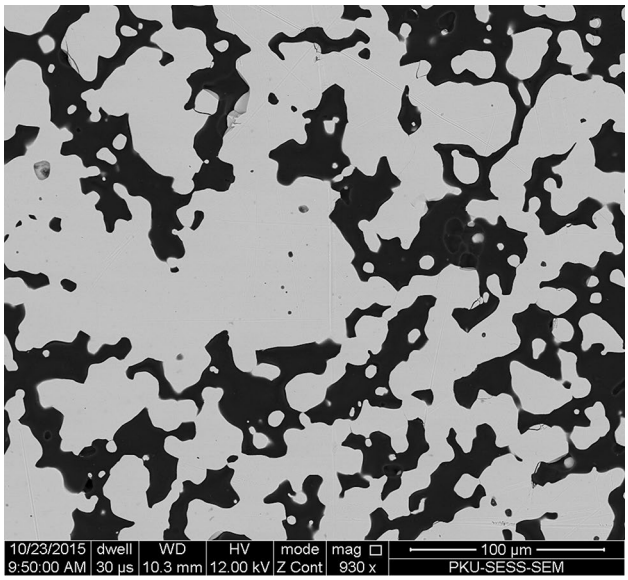

Fig. 1 Typical electron back-scatter image of synthetic Co_2TiO_4-Sp. The bright material is Co_2TiO_4-Sp, whereas the dark material is epoxy

Equation of state of Co_2TiO_4-Sp

Our DAC experiments (ambient T) were conducted up to ~24 GPa. The X-ray diffraction patterns obtained at pressures up to ~20.6 GPa do not show any apparent peak-broadening, peak-splitting, or new peak (Fig. 2), suggesting no phase transition up to this pressure. However, the X-ray diffraction patterns collected at pressures higher than ~22 GPa show significant peak-broadening and attained some new peaks which cannot be attributed to the cubic spinel structure. It follows that there must have been a phase transition somewhere between ~20.6 and 22 GPa. On the other hand, the major peaks of the X-ray diffraction pattern collected at ~24 GPa can be confidently assigned to the Co_2TiO_4-Sp still, indicating an incompletion of the phase transition. The new peaks can also be observed on decompression to 1 atm (Fig. 2).

The unit-cell parameters of the Co_2TiO_4-Sp at different pressures obtained during both compression and decompression are summarized in Table 1 and shown in Fig. 3a. During compression, the data obtained at $P > \sim 17$ GPa show some deviation from the trend defined by the data at lower pressures (Fig. 3a). Since the magnitude of this deviation is positively correlated with the nominal experimental P, we tentatively ascribe it to the progressive development of a non-hydrostatic condition in our DAC experiments. According to Klotz et al. (2009), our pressure medium, neon, should become incapable maintaining a quasi-hydrostatic

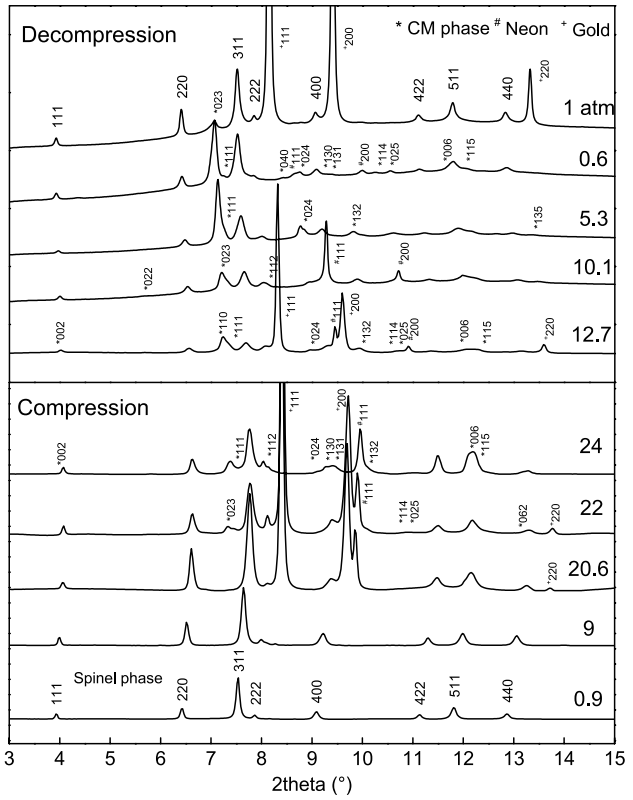

Fig. 2 Selected XRD patterns collected from compression (at 0.9, 9, 20.6, 22, 24 GPa) and decompression (at 12.7, 10.1, 5.3, 0.6 GPa and 1 atm) experiments (ambient *T*). The XRD peaks of neon were constantly observed as neon became a solid phase at high *P*, whereas those of gold were not. All other XRD peaks could be assigned to the Co_2TiO_4-Sp or Co_2TiO_4-CM, with the strong ones belonging to the former and the weak ones belonging to the latter. The X-ray peaks of the Co_2TiO_4-CM became evident at 22 GPa and were preserved throughout decompression

environment at $P > \sim 15$ GPa. Nevertheless, the volume data obtained from the compression and decompression experiments are well mixed, suggesting that the pressure status in our experiments was almost quasi-hydrostatic, and the elastic behavior of the Co_2TiO_4-Sp was fully reversible after compression to ~ 24 GPa.

To accurately determine the isothermal bulk modulus (K_T) of the Co_2TiO_4-Sp, we have only fitted the *P*–*V* data from the compression experiments collected at pressures from 1 atm to 17 GPa with the third-order Birch–Murnaghan equation of state (BM-EoS; Birch 1947) by a least-squares method:

$$P = \left(\frac{3}{2}\right)K_T\left[\left(\frac{V_0}{V}\right)^{\frac{7}{3}} - \left(\frac{V_0}{V}\right)^{\frac{5}{3}}\right] \times \left\{1 + \frac{3}{4}\left(K_T' - 4\right)\left[\left(\frac{V_0}{V}\right)^{\frac{2}{3}} - 1\right]\right\}, \quad (1)$$

Table 1 Experimentally determined unit-cell parameters of Co_2TiO_4-Sp at various pressures (room *T*)

P (GPa)	*a* (Å)	*V* (Å^3)
Compression		
0.0001	8.454(0)[a]	604.28(8)
0.9(1)[b]	8.443(0)	601.93(9)
1.7(1)	8.433(1)	599.61(12)
2.0(1)	8.427(1)	598.50(26)
2.3(1)	8.422(0)	597.28(6)
2.7(1)	8.416(0)	596.07(8)
3.1(1)	8.408(0)	594.39(9)
3.7(1)	8.401(1)	592.95(16)
4.3(1)	8.389(1)	590.43(17)
4.8(1)	8.383(1)	589.05(16)
5.1(1)	8.379(1)	588.27(19)
5.6(1)	8.373(1)	586.90(19)
6.4(1)	8.362(1)	584.61(13)
7.0(1)	8.348(1)	581.80(18)
8.0(1)	8.336(1)	579.30(15)
9.0(1)	8.319(1)	575.66(21)
10.0(1)	8.307(1)	573.22(18)
11.0(1)	8.292(1)	570.21(18)
11.5(1)	8.286(1)	568.88(30)
12.6(1)	8.275(2)	566.63(39)
13.5(1)	8.260(1)	563.56(22)
14.1(1)	8.255(1)	562.57(18)
15.0(1)	8.244(2)	560.81(38)
15.5(1)	8.237(1)	558.83(20)
16.5(1)	8.225(1)	556.50(18)
17.0(1)	8.220(1)	555.48(16)
16.7(1)	8.224(2)	556.14(34)
18.4(1)	8.209(1)	553.24(27)
19.2(1)	8.202(2)	551.71(34)
20.6(1)	8.192(2)	549.83(37)
22.0(1)	8.182(1)	547.75(25)
24.0(1)	8.167(4)	544.67(77)
Decompression		
21.7(1)	8.183(2)	548.04(38)
12.7(1)	8.271(2)	565.76(36)
10.1(1)	8.306(2)	573.05(35)
8.9(1)	8.320(2)	576.00(32)
5.3(1)	8.373(2)	586.98(34)
0.6(1)	8.449(2)	603.10(35)
0.2(1)	8.460(3)	605.42(63)
0.0001	8.459(2)	605.33(35)

[a]Numbers in parentheses representing one standard deviation

[b]Pressure determined by averaging the values measured before and after collection of synchrotron data; uncertainty of the *P* measurement in the high-*P* experiments assumed as 0.1 GPa

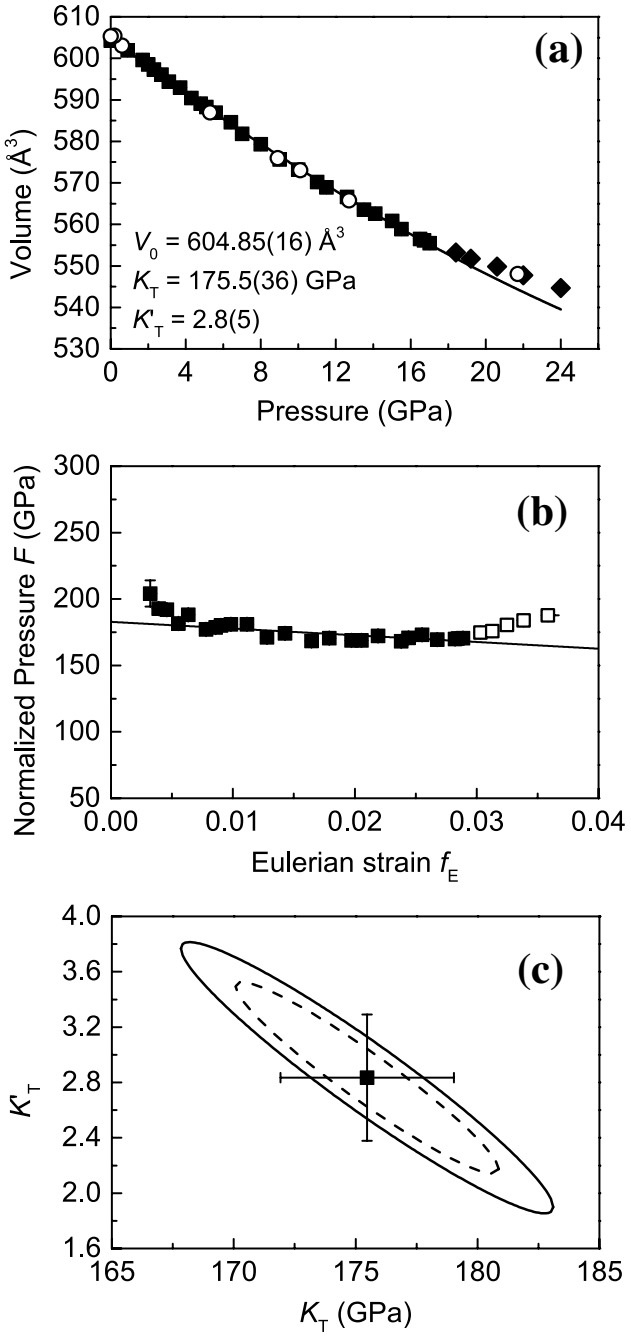

Fig. 3 **a** Pressure dependence of the volume for Co_2TiO_4-Sp (ambient T). The compressional data collected at pressures up to ~17 GPa and at pressures higher than ~17 GPa are represented by filled squares and filled diamonds, respectively (error bars equal to or smaller than the size of the symbols). The solid black curve is drawn according to our third-order BM-EoS (see text for the details). The decompressional data are represented by empty circles; **b** Eulerian strain-normalized pressure (f_E-F) plot for Co_2TiO_4-Sp. Estimated standard deviations have been calculated following the method in Heinz and Jeanloz (1984). Experimental data in the P ranges of below and above ~17 GPa are represented by filled and empty squares, respectively. The solid line with negative slope represents a weighted linear fit through the data in the P range from 1 atm to 17 GPa; **c** confidence ellipse in K_T and K'_T confirming our P–V data fit for Co_2TiO_4-Sp. The inner ellipse and outer ellipse are for a 68.3% confidence level (χ^2 distribution with 2 degrees of freedom $\Delta = 2.30$; see Angel 2000 for the details) and a 90% confidence level ($\Delta = 4.61$), respectively. The K_T and K'_T values obtained by the least-squares refinement (the software EoS fit 5.2; Angel 2000) are also shown. Error bars correspond to ± 1σ

Table 2 Isothermal bulk moduli (GPa) of Co_2TiO_4-Sp, Co_2TiO_4-CM and Co_2TiO_4-CT

Phase	K_T	K'_T	Method[a]	References
Sp	175.5(36)	2.8(5)	Exp/SX/Ne	This study
	167.2(12)	4(fixed)	Exp/SX/Ne	This study
	162(9)	–	Exp/US	Liebermann et al. (1977)
CM	161(7)	7.3(8)	Exp/SX/Ne	This study
	192.1(44)	4(fixed)	Exp/SX/Ne	This study
	138(3)	7.6(3)	Cal/DFT/GGA + PBE/usp	This study
	184(3)	4(fixed)	Cal/DFT/GGA + PBE/usp	This study
CT	196.8(14)	5.0(1)	Cal/DFT/GGA + PBE/usp	This study
	219.6(26)	4(fixed)	Cal/DFT/GGA + PBE/usp	This study

[a]Some details of the experimental techniques and simulating methods: *Exp* experimental, *Cal* calculated, *SX* synchrotron X-ray, *US* ultrasonic measurement, *Ne* pressure medium of Neon, *DFT* density functional theory, *GGA + PBE* generalized gradient approximation with Perdew–Burker–Ernzerhof functional, *usp* ultrasoft pseudopotential

where K'_T is the first pressure derivative of the K_T, and V_0 is the volume at zero pressure whereas V is the volume at high pressure. When the K'_T is set as 4, we obtain $K_T = 167.2(12)$ GPa, and $V_0 = 605.13(13)$ Å^3 for the Co_2TiO_4-Sp (Table 2). If the K'_T is not fixed, we obtain $K_T = 175.5(36)$ GPa, $K'_T = 2.8(5)$ and $V_0 = 604.85(16)$ Å^3 (Table 2).

The quality of the derived third-order BM-EoS for the Co_2TiO_4-Sp can be evaluated using the f_E–F plot (Fig. 3b). The Eulerian definition of the finite strain f_E is $f_E \equiv [(V_0/V)^{2/3}-1]/2$, and the normalized pressure F is $F \equiv P/[3f_E(1+2f_E)^{5/2}]$. Using F, the third-order BM-EoS can be rewritten as:

$$F = K_T + 3/2K_T(K'_T - 4)f_E, \quad (2)$$

so that the slope of the line defined by the experimental data should be equal to $3/2K_T(K'_T - 4)$, and the intercept value is the isothermal bulk modulus. Accordingly, a slope of zero implies $K'_T = 4$, a positive slope $K'_T > 4$, and a negative slope $K'_T < 4$. Figure 3b shows that the slope of the fitted line for the data in the P range from 1 atm to ~17 GPa is negative so that the value of the K'_T should be smaller than 4, confirming our EoS fit. Further, Fig. 3b shows that the data at $P > \sim 17$ GPa gradually deviate away from the line with negative slope defined by the data at lower pressures, suggesting that the spinel structure was increasingly strained indeed due to the progressive development of the non-hydrostatic pressure environment in our DAC experiments at $P > \sim 17$ GPa (Klotz et al. 2009).

A series of confidence ellipses in the K_T-K'_T space have been constructed (Bass et al. 1981; Fig. 3c) to evaluate the correlation between the K_T and K'_T obtained with the

compression data from 1 atm to ~17 GPa. The ellipses strongly elongate with negative slopes, indicating a negative correlation between the K_T and K_T' parameters. This observation implies that the experimental data can be fitted almost equally well by decreasing the value of K_T and increasing the value of K_T', or *vice versa*. In Fig. 3c, the area enclosed by the dashed line or solid line represents a 68.3% or 90% probability (or confidence level; Angel 2000) that the true values of K_T and K_T' lie in such an area, respectively. If we consider the 90% confidence ellipse, the K_T value can vary in the range from ~168 to ~183 GPa with the K_T' value from ~3.8 to ~1.9, which then verifies our data fitting process.

The adiabatic bulk modulus (K_S) of the Co_2TiO_4-Sp was once determined as 162(9) GPa using an ultrasonic pulse echo method (Table 2; Liebermann et al. 1977), about 7.7% smaller than our K_T value. According to Liu et al. (2016a), the K_S should be ~4 GPa larger than the K_T in any 4–2 spinel. The primary reason for the relatively small K_S is that the velocity data were taken at pressures up to 0.75 GPa only. As illustrated by Rigden et al. (1988) and Rigden and Jackson (1991), this magnitude of experimental pressure would have led to some underestimation of the porosity of the polycrystalline specimen, then some underestimation of the velocities, and eventually some underestimation of the K_S.

Structures of post-spinel phases

Our compression experiments have suggested that for the Co_2TiO_4 composition, a phase transition from the Co_2TiO_4-Sp to a new phase initiates at ~21 GPa. Since our compression experiments were conducted up to ~24 GPa only, where all the major XRD peaks belonged to the Co_2TiO_4-Sp, and only a few relatively weak XRD peaks were not attributable to the Co_2TiO_4-Sp (Fig. 2), the exact structure of this new phase could not be practically constrained by the experimental data. According to previous experimental studies (Errandonea 2014, and references therein), a number of structures such as the CM, CF, CT, TDS and ε-$MgAl_2O_4$ types are potential candidates. Using the most intense X-ray lines from the new phase [for example, the peak at ~7.1° (1 atm) or at ~7.4° (24 GPa)], we could narrow down the potential candidates to the following three types, the CM, CF and CT structures, but could not tell which one is the correct answer. These three structures have very similar powder XRD patterns (Yamanaka et al. 2008).

Theoretical simulation has been proved to be an effective method for determining the relative stabilities of different polymorphs (e.g., Zhang et al. 2017), and thus employed in this study. The calculated enthalpies of the Sp-fm, CM-fm, CF-fm, CT-fm, Sp-afm, CM-afm, CF-afm and CT-afm structures relative to that of the CF-afm structure for the P range of 0–50 GPa are shown in Fig. 4. Obviously, the Sp-afm has the lowest enthalpy from 0 to ~22 GPa, whereas the

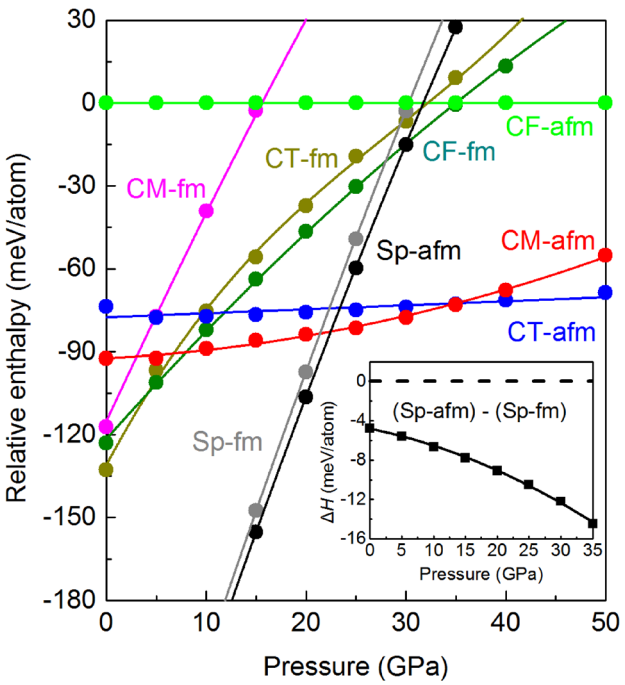

Fig. 4 Calculated enthalpies of Sp-fm, CM-fm, CF-fm, CT-fm, Sp-afm, CM-afm, CF-afm and CT-afm structures (Co_2TiO_4) relative to the enthalpy of the CF-afm for the P range of 0–50 GPa. To show the features clearly (especially the difference between the curve for the CM-afm and that for the CT-afm), we have chosen the CF-afm as the reference phase. The insert shows that the enthalpy difference between the Sp-fm and Sp-afm structures increases as P increases

CM-afm has the lowest enthalpy from ~22 to ~35 GPa. It follows that the new phase observed in our high-P experiments highly possibly adopts the CM structure. The experimentally observed XRD peaks for the new phase at 5.3 GPa, as summarized in Table 3, support the assignment of the CM structure to the new high-P phase, and the calculated transition P agrees well with the experimental observation. Moreover, the CT-afm attains the lowest enthalpy at $P > \sim 35$ GPa, meaning that the CM-afm might further transform to the CT-afm at a pressure somewhere close to ~35 GPa. This structural transition from the CM to CT phase is consistent with Yamanaka et al. (2008). Furthermore, the CF structure never attains the lowest enthalpy at any P, implying an insignificant role in the high-P behavior of the Co_2TiO_4 composition.

Pressure-induced magnetic transitions

A pressure-induced magnetic transition is usually accompanied by a volume reduction (e.g., Lin et al. 2013). For the Co_2TiO_4-Sp, no discernable volume reduction has been confidently observed in our room-T compression experiments (Fig. 3), implying no pressure-induced magnetic transition for this material. This conclusion has been substantiated by

Table 3 Experimentally observed XRD peaks for Co_2TiO_4-CM at ~5.3 GPa (room *T*)

h k l	d_{obs} (Å)	d_{calc} (Å)	d_{obs}–d_{calc} (Å)
0 0 2	4.86569	4.86549	0.00021
1 1 0	2.70137	2.70178	− 0.00040
0 2 3	2.66021	2.66043	− 0.00022
1 1 1	2.60290	2.60330	− 0.00039
1 1 2	2.36249	2.36204	0.00045
0 4 0	–		
0 2 4	2.15513	2.15561	− 0.00048
1 3 0	2.08766	2.08753	0.00013
1 3 1	–	–	–
1 3 2	1.91824	1.91841	− 0.00018
0 0 6	1.62184	1.62183	0.00002
1 1 5	1.57909	1.57915	− 0.00006
1 3 5	1.42377	1.42351	0.00026
1 5 3	–	–	–

The unit-cell parameters at 5.3 GPa were $a = 2.824(1)$ Å, $b = 9.301(9)$ Å, $c = 9.731(3)$ Å and $V = 255.55(18)$ Å^3

Table 4 Experimentally obtained unit-cell parameters of Co_2TiO_4-CM at various pressures (room *T*)

P (GPa)	*a* (Å)	*b* (Å)	*c* (Å)	*V* (Å^3)
Compression				
22.0(1)[a]	2.773(2)[b]	9.135(10)	9.419(3)	238.60(17)
24.0(1)	2.768(2)	9.120(10)	9.398(3)	237.22(17)
Decompression				
21.7(1)	2.774(2)	9.138(9)	9.433(3)	239.08(19)
12.7(1)	2.799(1)	9.224(9)	9.557(3)	246.75(18)
10.1(1)	2.806(1)	9.245(5)	9.617(3)	249.45(15)
8.9(1)	2.809(1)	9.263(9)	9.652(3)	251.19(17)
5.3(1)	2.824(1)	9.301(9)	9.731(3)	255.55(18)
0.6(1)	2.837(1)	9.358(8)	9.868(3)	261.93(16)

[a]Pressure determined by averaging the values measured before and after collection of synchrotron data; uncertainty of the *P* measurement in the high-*P* experiments assumed as 0.1 GPa

[b]Numbers in parentheses representing one standard deviation

our DFT calculation results; for the *P* interval from 0 to at least 35 GPa, the enthalpy of the Sp-afm is always lower than that of the Sp-fm (Fig. 4). We infer, therefore, that no pressure-induced magnetic transition may occur to the Co_2TiO_4-Sp material.

On the other hand, the enthalpy of the CM-fm phase is lower than that of the CM-afm phase at $P < \sim 3$ GPa, but higher at higher *P*; the enthalpy of the CT-fm phase is lower than that of the CT-afm phase at $P < \sim 10$ GPa, but higher at higher *P* (Fig. 4). As a result, pressure-induced magnetic transition might occur to the CM and CT structures. Our preliminary volume data experimentally obtained for the Co_2TiO_4-CM (to be shown in the next section), however, do not show any clear evidence of volume variation when the experimental *P* is decreased from higher than ~3 GPa to lower than ~3 GPa, probably suggesting no pressure-induced magnetic transition. Further experimentation is thus highly desirable to resolve this discrepancy.

Equation of state of Co_2TiO_4-CM and Co_2TiO_4-CT

The high-*P* unit-cell parameters of the Co_2TiO_4-CM obtained by our compression and decompression experiments are listed in Table 4 and shown in Fig. 5. It appears that the data collected during compression and decompression are well mixed, suggesting that the elastic behavior of the Co_2TiO_4-CM is by and large reversible, similar to the elastic behavior of the Co_2TiO_4-Sp. Further, all the unit-cell parameters vary non-linearly with *P* for the investigated *P* range from ~0.6 to 24 GPa, with the *a*-axis decreasing from 2.837(1) to 2.768(2) Å (by 2.4(1) %), the *b*-axis decreasing from 9.358(8) to 9.120(10) Å (by 2.5(1) %), the *c*-axis decreasing from 9.868(3) to 9.398(3) Å (by 4.76(4) %), and the volume decreasing from 261.93(16) to 237.22(17) Å^3 (by 9.4(1) %).

The experimental *P*–*V* data for the Co_2TiO_4-CM have been fitted to Eq. (1), yielding $V_0 = 263.0(3)$ Å^3, $K_T = 161(7)$ GPa and $K_T' = 7.3(8)$, or $V_0 = 262.2(3)$ Å^3 and $K_T = 192(4)$ GPa if K_T' is fixed as 4 (Table 2). A linearized third-order BM-EoS (Angel 2000) have been used to obtain the parameters of the equations of state for the crystallographic axes, yielding $a_0 = 2.840(1)$ Å and $K_{T-a} = 266(8)$ GPa for the *a*-axis, $b_0 = 9.362(6)$ Å and $K_{T-b} = 257(12)$ GPa for the *b*-axis, and $c_0 = 9.868(11)$ Å and $K_{T-c} = 119(5)$ GPa for the *c*-axis, if the K_{T-a}', K_{T-b}' and K_{T-c}' are fixed as 4. It follows that the Co_2TiO_4-CM has a prominent elastic anisotropy (K_{T-a}:K_{T-b}:K_{T-c} = ~2.24:2.16:1.00), with the *c*-axis as the most compressible axis. The compressibility of the *a*-axis is somehow very similar to that of the *b*-axis.

The calculated *P*–*V* data for the antiferromagnetic Co_2TiO_4-CM have been fitted to Eq. (1) as well, yielding $V_0 = 270.6(2)$ Å^3, $K_T = 138(3)$ GPa and $K_T' = 7.6(3)$, or $V_0 = 268.9(4)$ Å^3 and $K_T = 184(3)$ GPa with K_T' fixed as 4 (Table 2). These EoS parameters are in good agreement with our experimentally determined results if the uncertainty of the GGA method is considered (Zhang et al. 2016, 2017). The K_T' value of the Co_2TiO_4-CM is significantly larger than 4, indicating that the Co_2TiO_4-CM phase quickly attains large bulk modulus and becomes highly incompressible as *P* increases.

The calculated *P*–*V* data for the antiferromagnetic Co_2TiO_4-CT have been fitted to Eq. (1), yielding $V_0 = 264.6(1)$ Å^3, $K_T = 196.8(14)$ GPa and $K_T' = 5.0(1)$, or $V_0 = 263.6(3)$ Å^3 and $K_T = 219.6(26)$ GPa if K_T' is fixed as 4 (Table 2).

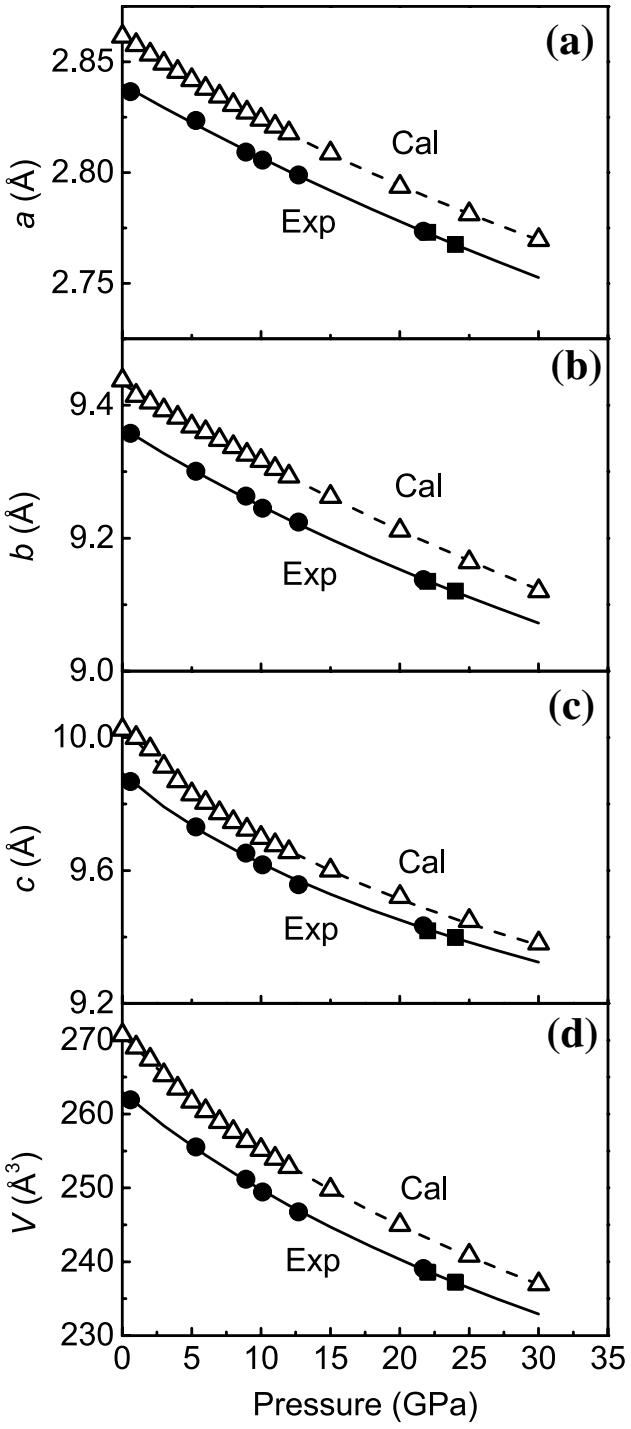

Fig. 5 Pressure dependence of the unit-cell parameters for the Co_2TiO_4-CM obtained by our experiment (labeled as "Exp") and DFT calculation (labeled as "Cal"; CM-afm structure): **a** the *a*-axis; **b** the *b*-axis; **c** the *c*-axis; **d** the volume. The compressional and decompressional data obtained by our high-*P* experiments are represented by filled squares and filled circles, respectively, while the calculated data are represented by empty triangles. The solid and broken curves are drawn according to the third-order BM-EoS parameters constrained with the experimentally obtained and theoretically calculated unit-cell parameters, respectively. In general, the slopes of the broken curves (theoretical) are slightly steeper than those of the solid curves (experimental), which is mostly attributable to the GGA method used in our simulation (small K_T underestimation)

The volume changes between the Co_2TiO_4-Sp phase and the Co_2TiO_4-CM phase, and between the Co_2TiO_4-CM phase and the Co_2TiO_4-CT phase are shown in Fig. 6. As for the first phase transition, the experimentally determined volume change is ~ 13.3% at ambient conditions or ~ 12.3% at the phase transition pressure. As for the second phase transition, the theoretically determined volume change is ~ 2.6% at ambient conditions or ~ 0.8% at the phase transition pressure.

Spinel and post-spinel phase assemblages at high *P* and high *T*

Akimoto and Syono (1967) has experimentally demonstrated that the Co_2TiO_4-Sp decomposes to a CoO-B1 (NaCl-type structure) + $CoTiO_3$-Ilm (ilmenite-type structure) phase assemblage at $P = \sim 2$–4 GPa and $T = \sim 1073$–1673 K. Further, Ito and Matsui (1979) has experimentally indicated that the $CoTiO_3$-Ilm decomposes to a CoO-B1 + TiO_2-α-PbO_2 (α-PbO_2-type structure) phase assemblage at ~ 20–25 GPa and 1273 K. It follows that the phase assemblage for the Co_2TiO_4 composition at some high *T* (1273 K for example) is presumably Co_2TiO_4-Sp ($P < \sim 2$–3 GPa), CoO-B1 + $CoTiO_3$-Ilm (~ 2–3 GPa < *P* < 20–25 GPa), and 2CoO-B1 + TiO_2-α-PbO_2 (*P* > 20–25 GPa) as *P* increases.

With the relevant data from Simons and Dachille (1967), Kidoh et al. (1984), Guo et al. (2002) and this study, the volume difference between the CoO-B1 + $CoTiO_3$-Ilm phase assemblage and the Co_2TiO_4-Sp, and between the 2CoO-B1 + TiO_2-α-PbO_2 phase assemblage and the Co_2TiO_4-Sp (ambient *P* and *T*) has been calculated as ~ 6.12 and ~ 8.20%, respectively.

Considering the volume difference between the Co_2TiO_4-Sp and the Co_2TiO_4-CM, ~ 13.3% at ambient *P* and *T* (Fig. 6a), the volume difference between the 2CoO-B1 + TiO_2-α-PbO_2 phase assemblage and the Co_2TiO_4-CM should be ~ 5.45% (ambient *P* and *T*). Consequently, it might be possible that at high *P*–*T* conditions, 2CoO-B1 + TiO_2-α-PbO_2 might recombine to form the Co_2TiO_4-CM. At still higher *P*, the Co_2TiO_4-CM might undergo a phase transition to the Co_2TiO_4-CT, as suggested by this study. It should be noted that a CT phase has been demonstrated for some A_2TiO_4-Sp including the Fe_2TiO_4-Sp and Zn_2TiO_4-Sp (Wang et al. 2002; Yamanaka et al. 2009; Zhang et al. 2017).

The formation of a post-spinel phase (as the Co_2TiO_4-CM in this study) from the oxides (CoO-B1 and TiO_2-α-PbO_2) resulted from the breakdown reaction of an A_2TiO_4-Sp (Co_2TiO_4-Sp) is very interesting, and leads to a tantalizing question: is there a thermodynamically stable post-spinel phase with the Mg_2SiO_4 composition in the lower mantle of the Earth? Numerous studies have suggested that under equilibrium conditions, the Mg_2SiO_4-Sp (ringwoodite) should decompose to the phase assemblage of bridgmanite (perovskite-type

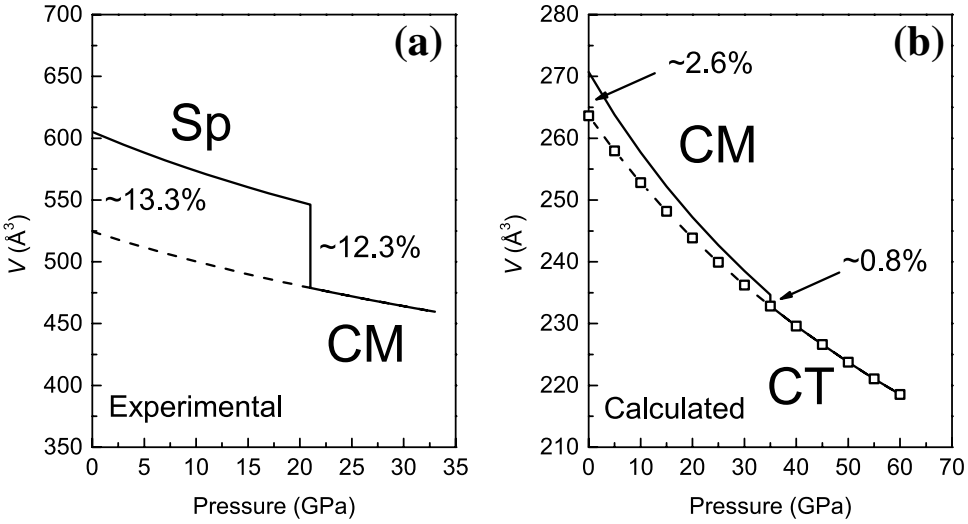

Fig. 6 Volume change between Co_2TiO_4-Sp and Co_2TiO_4-CM phases (**a**), and between antiferromagnetic Co_2TiO_4-CM and Co_2TiO_4-CT phases (**b**). The high-*P* volumes in **a** and **b** are obtained by our compression experiments and theoretical calculations, respectively. Note that the calculated volumes of Co_2TiO_4-CT at different pressures are represented by empty squares. The volume change at the ambient and transition pressure is defined as $\Delta V\,(\%) = (V_1 - V_2)/V_1 \times 100$, where 1 and 2 stand for low-*P* and high-*P* phase, respectively

$MgSiO_3$; $MgSiO_3$-Pv) + periclase (rock salt-type structure; MgO-Rs) at the boundary between the upper and lower mantle of the Earth, which should further turn into the phase assemblage of post-perovskite ($MgSiO_3$-PPv) + MgO-Rs at the base of the lower mantle (e.g., Liu 1976; Murakami et al. 2004; Oganov and Ono 2004; Tsuchiya et al. 2004). In other words, no stable post-spinel of the Mg_2SiO_4 composition has been observed for the lower mantle so far. Considering the difficulty in performing experiments at these challenging *P*-*T* conditions, however, the fore-mentioned phase assemblages should be viewed with great caution, and further examined as the high-*P* experimental techniques advance with time. By performing more experiments, for example, Zhang et al. (2014) recently demonstrated for the lower mantle an Fe-rich hexagonal phase which had never been experimentally detected ever before. Moreover, some new investigations have suggested that some metastable post-spinel structures exist for the Mg_2SiO_4 composition at very low temperatures up to the ambient *T* (Finkelstein et al. 2014; Zhou et al. 2015). Further studies are clearly required to examine the metastability (or stability) of these post-spinel structures and their relations to other phases or phase assemblages in the vast *P*–*T* space of the lower mantle before a sound answer can be reached.

Bulk moduli of A_2TiO_4-Sp

The bulk moduli of some other A_2TiO_4-Sp such as the Fe_2TiO_4-Sp, Mg_2TiO_4-Sp and Zn_2TiO_4-Sp have been investigated by the DAC + synchrotron radiation experimental technique as well (e.g., Yamanaka et al. 2009, 2013; Xiong et al. 2015; Lv et al. 2016; Zhang et al. 2017). As shown in Fig. 7, a very good linear relationship is defined by the V_0–K_T data of the Co_2TiO_4-Sp, Mg_2TiO_4-Sp and Zn_2TiO_4-Sp:

$$K_T = 2054(58) - 3.1(1)V_0, \quad (3)$$

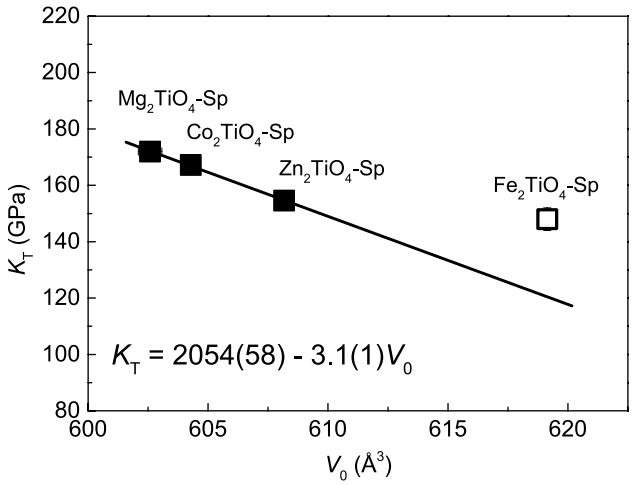

Fig. 7 V_0–K_T relationship of some titanate spinels (K_T' fixed as 4). Data sources are Xiong et al. (2015; K_T = 148(4) GPa), Lv et al. (2016; K_T = 172(1) GPa), Zhang et al. (2017; K_T = 154.6(12) GPa) and this study

where K_T is in GPa and V_0 in Å^3 (K_T' fixed as 4). Somehow the K_T of the Fe_2TiO_4-Sp obtained by Xiong et al. (2015) shows significant deviation.

All A_2TiO_4-Sp have an inverse spinel structure, $(A^{2+})^{tet}(A^{2+}Ti^{4+})^{oct}O_4$, with the A cations on the tetrahedral sites in fourfold coordination (IV) and those on the octahedral sites in sixfold coordination (VI). The correlation between the radius of the cation in the fourfold or sixfold coordination (denoted as r_{0-tet} and r_{0-oct}, respectively) and K_T at ambient conditions for the Co_2TiO_4-Sp, Fe_2TiO_4-Sp, Mg_2TiO_4-Sp and Zn_2TiO_4-Sp is shown in Fig. 8. The K_T values seemingly decrease linearly with the r_{0-oct}:

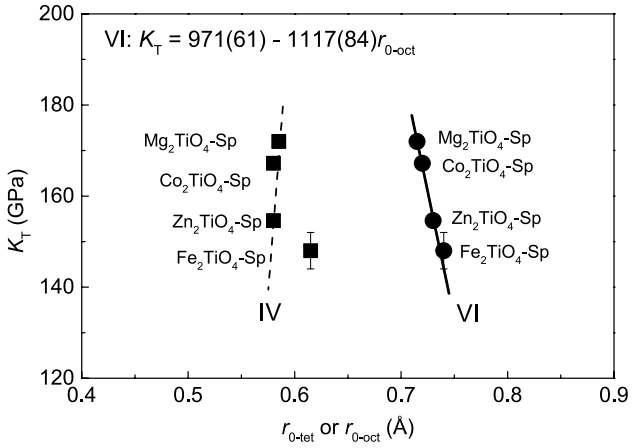

Fig. 8 Relationships of $r_{0-\mathrm{oct}}$–K_T (filled circles, labeled as "VI") and $r_{0-\mathrm{tet}}$–K_T (filled squares, labeled as "IV") of some titanate spinels ($K_\mathrm{T}^{'}$ fixed as 4). The cation radii are from O'Neill and Navrotsky (1983), whereas the K_T values are from Xiong et al. (2015), Lv et al. (2016), Zhang et al. (2017) and this study

$$K_\mathrm{T} = 971(61) - 1117(84)r_{0-\mathrm{oct}}, \quad (4)$$

where K_T is in GPa and $r_{0-\mathrm{oct}}$ in Å ($K_\mathrm{T}^{'}$ fixed as 4). The nearly vertical trend defined by the $r_{0-\mathrm{oct}}$–K_T data suggests a significant effect on the K_T for the cation substitution on the octahedral sites, in good agreement with Hazen and Yang (1999), Lv et al. (2016) and Liu et al. (2016b). On the other hand, the $r_{0-\mathrm{tet}}$–K_T data demonstrate a more complicated pattern: the data for the Co_2TiO_4-Sp, Mg_2TiO_4-Sp and Zn_2TiO_4-Sp appear more or less on a straight line (with a positive slope though), but those for the Fe_2TiO_4-Sp show large deviation.

The significant deviations of the V_0–K_T and $r_{0-\mathrm{tet}}$–K_T data for the Fe_2TiO_4-Sp from the trends defined by those of other three A_2TiO_4-Sp might be ascribed to the Jahn–Teller effect of Fe^{2+} at the tetrahedral sites. Although the Jahn–Teller effect has been well explored on the high-P phase transition of the Fe_2TiO_4-Sp (Yamanaka et al. 2009, 2013), its influence on the K_T of the Fe_2TiO_4-Sp is still unknown so that more investigation on the Jahn–Teller effect in the Fe_2TiO_4-Sp is deemed necessary.

Acknowledgements We thank two anonymous reviewers for their constructive comments on our manuscript, and Dr. T. Tsuchiya for his criticizing comments on and his editorial handling of our paper. The high-P work was performed at GeoSoilEnviroCARS (Sector 13), Advanced Photon Source (APS), Argonne National Laboratory. GeoSoilEnviroCARS is supported by the National Science Foundation-Earth Sciences (EAR-1128799) and Department of Energy-Geo-Sciences (DE-FG02-94ER14466). Use of the COMPRES-GSECARS gas loading system was supported by COMPRES under NSF Cooperative Agreement EAR 11-57758 and by GSECARS through NSF Grant EAR-1128799 and DOE Grant DE-FG02-94ER14466. This research used resources of the Advanced Photon Source, a US Department of Energy (DOE) Office of Science User Facility operated for the DOE Office of Science by Argonne National Laboratory under Contract No. DE-AC02-06CH11357. Financially, this study was supported by the Strategic Priority Research Program (B) of Chinese Academy of Sciences (Grant No. XDB18000000), by the DREAM project of MOST, China (Grant No. 2016YFC0600408), and by the Natural Sciences and Engineering Research Council of Canada.

References

Akimoto S, Syono Y (1967) High-pressure decomposition of some titanate spinels. J Chem Phys 47:1813–1817

Angel RJ (2000) Equation of state. In: Hazen RM, Downs RT (eds) High-temperature and high-pressure crystal chemistry. Reviews in Mineralogy and Geochemistry, vol 41. Mineralogical Society of America, Chantilly, pp 35–60

Bass JD, Liebermann RC, Weidner DJ, Finch SJ (1981) Elastic properties from acoustic and volume compression experiments. Phys Earth Planet Int 25:140–158

Bertaut EF, Blum P (1956) Détermination de la structure de Ti_2CaO_4 par la Méthode Self-Consistante d'Approche Directe. Acta Cryst 9:121–126

Birch F (1947) Finite elastic strain of cubic crystals. Phys Rev 71:809–924

Decker BF, Kasper JS (1957) The structure of calcium ferrite. Acta Cryst 10:332–337

Dube GR, Darshane VS (1991) X-ray, electrical and catalytic studies of the system $CoFe_2O_4$-Co_2TiO_4. Bull Chem Soc Jpn 64:2449–2453

Dudarev SL, Botton GA, Savrasov SY, Humphreys CJ, Sutton AP (1998) Electron-energy-loss spectra and the structural stability of nickel oxide: An LSDA + U study. Phys Rev B 57:1505

Errandonea D (2014) AB_2O_4 compounds at high pressures. In: Manjon FJ, Tiginyanu I, Ursaki V (eds) Pressure-induced phase transitions in AB_2X_4 chalcogenide compounds, vol 189. Springer, New York, pp 55–62

Finkelstein GJ, Dera PK, Jahn S, Oganov AR, Holl CM, Meng Y, Duffy TS (2014) Phase transitions and equation of state of forsterite to 90 GPa from single-crystal X-ray diffraction and molecular modeling. Am Mineral 99:35–43

Frost DJ (2008) The upper mantle and transition zone. Elements 4:171–176

Giesber HG, Pennington WT, Kolis JW (2001) Redetermination of $CaMn_2O_4$. Acta Cryst 57:329–330

Guo Q, Mao HK, Hu J, Shu J, Hemley RJ (2002) The phase transitions of CoO under static pressure to 104 GPa. J Phys Condens Matter 14:11369–11374

Hagenmuller P, Guillaud C, Lecerf A, Rault M, Villers G (1966) Préparation, étude cristallographique et magnétique de quelques séries d'oxydes à structure spinelle de formule $Mn_{1+x}M_{2(1-x)}Ti_xO_4$. Bull Soc Chim Fr 8:2589–2596

Hazen RM, Yang H (1999) Effects of cation substitution and order-disorder on P-V-T equations of state of cubic spinels. Am Mineral 84:1956–1960

He Q, Liu X, Hu X, Deng L, Chen Z, Li B, Fei Y (2012) Solid solutions between lead fluorapatite and lead fluorvanadate apatite: compressibility determined using a diamond-anvil cell coupled with synchrotron X-ray diffraction. Phys Chem Mineral 39:219–226

Heinz DL, Jeanloz R (1984) The equation of state of the gold calibration standard. J Appl Phys 55:885–893

Hirota K, Inoue T, Mochida N, Ohtsuka A (1990) Study of germanium spinels (part 3). J Ceram Soc Jpn 98:976–986

Hohenberg P, Kohn W (1964) Inhomogeneous electron gas. Phys Rev 136:864–871

Holland TJB, Redfern SAT (1997) Unit cell refinement from powder diffraction data: the use of regression diagnostics. Mineral Magn 61:65–77

Irifune T, Ringwood AE (1987) Phase transformation in primitive MORB and pyrolite compositions to 25 GPa and some geophysical implications. In: Manghnani M, Syono Y (eds) High-pressure research in mineral physics. Terra/American Geophys Union, Tokyo/Washington, pp 221–230

Ita J, Stixrude L (1992) Petrology, elasticity and composition of the mantle transition zone. J Geophys Res 97:6849–6866

Ito E, Matsui Y (1979) High-pressure transformations in silicates, germinates and titanates with ABO_3 stoichiometry. Phys Chem Mineral 4:265–273

Kidoh K, Tanaka K, Marumo F (1984) Electron density distribution in an ilmenite-type crystal of cobalt(II) titanium(IV) trioxide. Acta Cryst B40:92–96

Klotz S, Chervin JC, Munsch P, Le Marchand G (2009) Hydrostatic limits of 11 pressure transmitting media. J Phys D Appl Phys 42:075413

Kohn W, Sham LJ (1965) Self-consistent equations including exchange and correlation effects. Phys Rev 140:1133–1138

Kresse G, Hafner J (1994) Norm-conserving and ultrasoft pseudopotentials for first-row and transition elements. J Phys-Condens Mater 6:8245–8257

Liebermann RC, Jackson I, Ringwood AE (1977) Elasticity and phase equilibria of spinel disproportionation reactions. Geophys J R Astron Soc 50:553–586

Lin JF, Speziale S, Mao Z, Marquardt H (2013) Effects of the electronic spin transitions of iron in lower mantle minerals: implications for deep mantle geophysics and geochemistry. Rev Geophys 51:244–275

Liu L (1976) The post-spinel phases of forsterite. Nature 262:770–772

Liu X, Shieh SR, Fleet ME, Zhang L, He Q (2011) Equation of state of carbonated hydroxylapatite at ambient temperature up to 10 GPa: significance of carbonate. Am Mineral 96:74–80

Liu X, Xiong Z, Chang L, He Q, Wang F, Shieh SR, Wu C, Li B, Zhang L (2016a) Anhydrous ringwoodites in the mantle transition zone: their bulk modulus, solid solution behavior, compositional variation, and sound velocity feature. Solid Earth Sci 1:28–47

Liu X, Xiong Z, Shieh SR, He Q, Deng L, Zhang Y, Chang L, Wang F, Hong X, Chen Z (2016b) Non-monotonic compositional dependence of isothermal bulk modulus of the $(Mg_{1-x}Mn_x)Cr_2O_4$ spinel solid solutions, and its origin and implication. Solid Earth Sci 1:89–100

Lv M, Liu X, Shieh SR, Xie T, Wang F, Prescher C, Prakapenka VB (2016) Equation of state of synthetic qandilite Mg_2TiO_4 at ambient temperature. Phys Chem Mineral 43:301–306

Mao HK, Bell PM, Shaner JW, Steinberg DJ (1978) Specific volume measurements of Cu, Mo, Pt, and Au and calibration of ruby R1 fluorescence pressure gauge for 0.006 to 1 Mbar. J Appl Phys 49:3276–3283

Millard RL, Peterson RC, Hunter BK (1995) Study of the cubic to tetragonal transition in Mg_2TiO_4 and Zn_2TiO_4 spinels by ^{17}O MAS NMR and rietveld refinement of X-ray diffraction data. Am Mineral 80:885–896

Monkhorst HJ, Pack JD (1976) Special points for Brillouin-zone integrations. Phys Rev B 13:5188–5192

Murakami M, Hirose K, Kawamura K, Sata N, Ohishi Y (2004) Post-perovskite phase transition in $MgSiO_3$. Science 304:855–858

O'Neill HSTC, Navrotsky A (1983) Simple spinels: crystallographic parameters, cation radii, lattice energies, and cation distribution. Am Mineral 68:181–194

Oganov AR, Ono S (2004) Theoretical and experimental evidence for a post-perovskite phase of $MgSiO_3$ in Earth's D" layer. Nature 430:445–448

Payne MC, Teter MP, Allan DC, Arias TA, Joannopoulos JD (1992) Iterative minimization techniques for ab initio total-energy calculations: molecular dynamics and conjugate gradients. Rev Mod Phys 64:1045–1097

Perdew JP, Burke K, Ernzerhof M (1996) Generalized gradient approximation made simple. Phys Rev Lett 77:3865–3868

Prescher C, Prakapenka VB (2015) DIOPTAS: a program for reduction of two-dimensional X-ray diffraction data and data exploration. High Pressure Res 35:223–230

Prosnikov MA, Molchanova AD, Dubrovin RM, Boldyrev KN, Smirnov AN, Davydov VY, Balbashov AM, Popova MN, Pisarev RV (2016) Lattice dynamics and electronic structure of cobalt–titanium spinel Co_2TiO_4. Phys Solid State 58:2516–2522

Rankin RB, Campos A, Tian H, Siriwardane R, Roy A, Spivey JJ, Sholl DS, Johnson JK (2008) Characterization of bulk structure in zinc orthotitanate: a density functional theory and EXAFS investigation. J Am Ceram Soc 91:584–590

Rigden SM, Jackson I (1991) Elasticity of germanate and silicate spinels at high pressure. J Geophys Res 96:9999–10006

Rigden SM, Jackson I, Niesler H, Ringwood AE, Liebermann RC (1988) Pressure dependence of the elastic wave velocities from Mg_2GeO_4 spinel to 3 GPa. Geophys Res Lett 15:605–608

Ringwood AE, Reid AF (1968) High pressure transformations of spinels (I). Earth Planet Sci Lett 5:245–250

Romeijn FC (1953) Physical and crystallographical properties of some spinels. Philips Res Rep 8:304–320

Sakamoto N (1962) Magnetic properties of cobalt titanate. J Phys Soc Jpn 17:99–102

Sedler IK, Feenstra A, Peters T (1994) An X-ray powder diffraction study of synthetic $(Fe, Mn)_2TiO_4$ spinel. Eur J Mineral 6:873–885

Simons PY, Dachille F (1967) The structure of TiO_2 II, a high-pressure phase of TiO_2. Acta Cryst 23:334–336

Tsuchiya T, Tsuchiya J, Umenoto K, Wentzcovitch RM (2004) Phase transition in $MgSiO_3$ perovskite in the Earth's lower mantle. Earth Planet Sci Lett 224:241–248

Vanderbilt D (1990) Soft self-consistent pseudopotentials in a generalized eigenvalue formalism. Phys Rev B 41:7892–7895

Verwey EJW, Heilmann EL (1947) Physical properties and cation arrangement of oxides with spinel structures I. cation arrangement in spinels. J Chem Phys 15:174–180

Wang Z, Saxena SK, Zha CS (2002) In situ X-ray diffraction and Raman spectroscopy of pressure-induced phase transformation in spinel Zn_2TiO_4. Phys Rev B 66:024103

Wechsler BA, Von Dreele RB (1989) Structure refinements of Mg_2TiO_4, $MgTiO_3$ and $MgTi_2O_5$ by time-of-flight neutron powder diffraction. Acta Cryst B 45:542–549

Xiong Z, Liu X, Shieh SR, Wang F, Wu X, Hong X, Shi Y (2015) Equation of state of a synthetic ulvöspinel, $(Fe_{1.94}Ti_{0.03})Ti_{1.00}O_{4.00}$, at ambient temperature. Phys Chem Mineral 42:171–177

Yamanaka T, Uchida A, Nakamoto Y (2008) Structural transition of post-spinel phases $CaMn_2O_4$, $CaFe_2O_4$, and $CaTi_2O_4$ under high pressures up to 80 GPa. Am Mineral 93:1874–1881

Yamanaka T, Mine T, Asogawa S, Nakamoto Y (2009) Jahn-Teller transition of Fe_2TiO_4 observed by maximum entropy method at high pressure and low temperature. Phys Rev B 80:134120

Yamanaka T, Kyono A, Nakamoto Y, Meng Y, Kharlamova S, Struzhkin VV, Mao HK (2013) High-pressure phase transitions of $Fe_{3-x}Ti_xO_4$ solid solution up to 60 GPa correlated with electronic spin transition. Am Mineral 98:736–744

Zhang L, Meng Y, Yang W, Wang L, Mao WL, Zeng QS, Jeong JS, Wagner AJ, Mkhoyan KA, Liu W, Xu R, Mao HK (2014) Disproportionation of $(Mg,Fe)SiO_3$ perovskite in Earth's deep lower mantle. Science 344:877–882

Zhang Y, Liu X, Xiong Z, Zhang Z (2016) Compressional behavior of $MgCr_2O_4$ spinel from first-principles simulation. Sci Chin Earth Sci 59:989–996

Zhang Y, Liu X, Shieh SR, Bao X, Xie T, Wang F, Zhang Z, Prescher C, Prakapenka VB (2017) Spinel and post-spinel phase assemblages in Zn_2TiO_4: an experimental and theoretical study. Phys Chem Mineral 44:109–123

Zhou P, Wu G, Zuo C, Li L, Zheng Z, Zhang W, Pan G, Wang F (2015) Study on electronic structures and mechanical properties of new predicted orthorhombic Mg_2SiO_4 under high pressure. J Alloys Compd 630:11–22